TNF-α and IL-10 Control CXCL13 Expression in Human Macrophages

Nessrine Bellamri, Roselyne Viel, Claudie Morzadec, Valérie Lecureur, Audrey Joannes, Bertrand de Latour, Francisco Llamas-Gutierrez, Lutz Wollin, Stéphane Jouneau, Laurent Vernhet

TNF-α and IL-10 control CXCL13 expression in human macrophages

Nessrine Bellamri[1], Roselyne Viel[2], Claudie Morzadec[1], Valérie Lecureur[1], Audrey Joannes[1], Bertrand de Latour[3], Francisco Llamas-Gutierrez[4], Lutz Wollin[5], Stéphane Jouneau[6, 7,*] and Laurent Vernhet[1, #,*]

[1]Univ Rennes, Inserm, EHESP, Irset (Institut de recherche en santé, environnement et travail) - UMR_S 1085, F-35000 Rennes, France

[2] H2P2, Histopathological Platform, Univ Rennes, F-35000 Rennes, France

[3]Service de Chirurgie cardio-thoracique et vasculaire, Centre Hospitalier Universitaire, Rennes, France

[4]Service d'anatomopathologie, Centre Hospitalier Universitaire, Rennes, France

[5]Boehringer Ingelheim Pharma GmbH & Co, KG, Biberach an der Riss, Germany

[6]Univ Rennes, CHU Rennes, Inserm, EHESP, Irset (Institut de recherche en santé, environnement et travail) - UMR_S 1085, F-35000 Rennes, France

[7]Service de Pneumologie, Centre de compétences pour les maladies pulmonaires rares de Bretagne, Centre Hospitalier Universitaire, Rennes, France

[#]LV and SJ contributed equally

Running title: Macrophage CXCL13 expression and idiopathic lung fibrosis

[*]**Corresponding author**: Laurent Vernhet, Univ. Rennes, Inserm, EHESP, Irset (Institut de recherche en santé, environnement et travail) - UMR_S 1085, F-35000 Rennes, France. Phone: 33-2-23-23-48-07; Fax: 33-2-23-23-47-94. Email: laurent.vernhet@univ-rennes1.fr

Abbreviations: ILD: interstitial lung disease, IPF: idiopathic pulmonary fibrosis, IF: immunofluorescence, MoDM: blood monocyte-derived macrophages, AM: alveolar macrophages, M-CSF: macrophage colony-stimulating factor, BAL: bronchoalveolar

lavages, LPS: lipopolysaccharide, IHC: immunohistochemistry, IF: immunofluorescence, TNF-α: tumor necrosis factor-α (TNF-α), IL: interleukin, Ab: antibody; LOQ: limit of quantification, TNFR2: TNF-α receptor 2

Abstract

The chemokine CXCL13 controls the normal organization of secondary lymphoid tissues and the neogenesis of ectopic lymphoid structures in nonlymphoid organs, particularly the lungs. The progression and severity of idiopathic pulmonary fibrosis (IPF), a fatal and irreversible interstitial lung disease, is predicted by the circulating blood concentrations of CXCL13. While CXCL13 is produced by pulmonary tissues, it has not been determined which cells are involved. This study examines CXCL13 production by lung tissue macrophages from patients with IPF and the signaling pathways controlling CXCL13 gene expression in human alveolar macrophages (AM) and monocyte-derived macrophages (MoDM). CXCL13 is found in CD68- and CD206-positive AM from patients with IPF, and the CXCL13 gene is induced in these macrophages and MoDM when they are stimulated with lipopolysaccharide. We found that TNF-α and IL-10 control optimal CXCL13 gene expression in MoDM and possibly in AM by activating the NF-κB and JAK/STAT pathways, respectively. We also found that blood TNF-α and CXCL13 concentrations are significantly correlated in patients with IPF, suggesting that TNF-α contributes to CXCL13 production in humans. In conclusion, the results of this study demonstrate that AM from patients with IPF produces CXCL13 and that the NF-κB and JAK/STAT pathways are required to induce the expression of this major chemokine.

Key points

- CXCL13 is expressed in alveolar macrophages from patients with IPF
- TNF-α and IL-10 control CXCL13 expression through NF-κB and JAK/STAT, respectively

Keywords: CXCL13, macrophage, idiopathic lung fibrosis, TNF-α, IL-10, NF-κB

Introduction

The chemokine CXCL13, also known as B lymphocyte chemoattractant and B cell attracting chemokine-1, controls the normal organization of secondary lymphoid tissues by stimulating the homing of B and follicular T helper lymphocytes (1). CXCL13 is constitutively expressed in these structures and is mainly produced by follicular dendritic cells and stromal cells in response to lymphotoxin-β (1). CXCL13 also promotes the neogenesis of ectopic lymphoid structures in nonlymphoid organs (1), especially in chronic inflammatory diseases, such as ulcerative colitis and chronic obstructive pulmonary disease, and in autoimmune diseases, such as rheumatoid arthritis and systemic lupus erythematosus (2–5). Follicular dendritic cells and stromal cells do not produce CXCL13 in ulcerative colitis and rheumatoid arthritis lesions, but macrophages within the lymphoid structures may produce CXCL13 (2).

Recent studies have demonstrated that CXCL13 is also a robust prognostic biomarker of idiopathic pulmonary fibrosis (IPF), a progressive, fatal interstitial lung disease (ILD) (6–8). Blood CXCL13 concentrations of patients with IPF are significantly elevated, and they predict the severity and progression of the disease (6). The concentrations of CXCL13 mRNA in pulmonary tissues from patients with IPF are significantly increased, and CXCL13 protein is abundant around or within the B-cell aggregates near the fibrotic tissues (6, 7). However, the cellular source of CXCL13 in lung tissues has not been determined.

Pulmonary macrophages play a pivotal role in IPF by secreting a variety of pro-inflammatory and pro-fibrotic mediators that promote the recruitment of immune cells and the activation and differentiation of lung fibroblasts (9, 10). Most alveolar macrophages (AMs) of healthy subjects come from self-renewing fetal monocytes (11). In contrast, chronic exposure to aggressive biological or chemical agents triggers the recruitment of circulating blood monocytes that differentiate into interstitial macrophages and/or AM in the lungs (10). Blood

monocyte-derived macrophages (MoDMs) are intimately involved in the development of lung fibrosis in murine models. The genetic deletion of blood monocyte-derived AM and the selective depletion of $Ly6C^{hi}$ circulating monocytes significantly inhibit the development of bleomycin-induced lung fibrosis in mice (12, 13). Macrophage colony-stimulating factor (M-CSF), which stimulates blood monocytes to differentiate into macrophages, favors the development of lung fibrosis in these mice (14). Bleomycin-treated $M\text{-}CSF^{-/-}$ mice have fewer AM than normal and a lower fibrotic score than wild-type mice (14). Several indicators suggest that human blood MoDM, potentially differentiated by M-CSF, also contributes to the development of lung fibrosis. The concentration of M-CSF in bronchoalveolar lavages (BAL) and the density of CD68-positive cells (macrophage lineage) in the pulmonary tissues of patients with IPF are significantly higher than in control subjects (14, 15). Using flow cytometry, Yu et al. (2016) demonstrated that most interstitial macrophages and AM from patients with IPF strongly bear the CD206 mannose receptor, whose expression is potently induced by M-CSF during human blood monocyte differentiation (16, 17). Finally, human MoDM, differentiated *in vitro* with M-CSF, produces CXCL13 when stimulated with lipopolysaccharide (LPS) (2). Taken together, these findings suggest that human pulmonary macrophages can produce CXCL13. The present study was thus designed to assess this hypothesis.

First, we used immunohistochemistry (IHC) and immunofluorescence (IF) to characterize CXCL13 production by macrophages in lung tissues isolated from patients with IPF. Next, we identified the cytokines and signaling pathways regulating *in vitro* CXCL13 expression in human MoDM and AM. Last, we assessed the relationship between the circulating concentrations of these cytokines and CXCL13 in humans suffering from IPF.

Materials and Methods

Chemicals and reagents

M-CSF was purchased from Miltenyi Biotec (Paris, France). Lipopolysaccharide (LPS) (*Escherichia* coli O55:B5) and BAY-117082 (BAY) were from Sigma-Aldrich (Saint-Quentin Fallavier, France). Tumor necrosis factor-α (TNF-α) and interleukin (IL)-10 were obtained from PeproTech (Neuilly-sur-Seine, France); anti-TNF-α and anti-IL-10 neutralizing antibodies (Abs) were provided by R&D System Europe (Biotechne, Lille, France); anti-phospho-IκBα (ser32), anti-IκBα, anti-p100/p52, anti-RelB, anti-phospho-STAT3 (Tyr705) and anti-GAPDH primary Abs were from Cell Signaling Technology (Ozyme, Montigny-le Bretonneaux, France). Ruxolitinib was provided by Selleckchem (Houston, TX, USA). Si-RNAs: ON-TARGETplus Control pool Nontargeting Pool (D-001810-10-05, Si-CTR), ON-TARGETplus Human RelB siRNA-SMARTpool (L-004767-00-0005, Si-BelB) and ON-TARGETplus Human NFκB2 siRNA-SMARTpool (L-003918-00-0005, Si-p100/p52) were purchased from Dharmacon (Horizon Discovery, UK).

Immunohistochemistry

Lung biopsy samples were obtained from six patients with IPF. IPF was diagnosed according to the 2011 ATS/ERS/JRS/ALAT criteria, which include histopathological features of usual interstitial pneumonia (18). Clinical and pulmonary functional data of the six subjects are presented in Table S1 (see "Lung biopsies"). This study was approved by the Rennes University Hospital Ethics Committee (Comité d'éthique, avis n°16.123). Written informed consent was obtained from all subjects. Serial sections (4 µm) were cut from paraffin-embedded tissue, mounted on positively charged slides and dried at 58°C for 60 min. The sections were immunostained in the Discovery Automated IHC stainer (Ventana Medical Systems, Tucson, AZ) using DABMap kits or CHROMOMap DAB kits to detect CD20,

CD68 and CD206 or CXCL13, respectively. Briefly, paraffin was removed with EZ Prep solution (8 min / 75 °C), and antigens were retrieved by incubation in CC1Tris-based buffer (95-100 °C / 60 min). Endogenous peroxidase was blocked by incubation with Inhibitor-D 3% H_2O_2 (Ventana) (37°C / 4 min). Sections were then rinsed and incubated (37°C / 60 min) with primary Abs: mouse monoclonal anti-CD20 (Dako, M0755, clone L26, diluted 1/600), mouse monoclonal anti-CD68 (M0876, clone PG-M1, DAKO, diluted 1/1000), rabbit polyclonal anti-CD206 (Abcam, ab64693, diluted 1/2000), or mouse monoclonal anti-CXCL13 (R&D System, AF801, diluted 1/500). Signals were enhanced with compatible biotinylated goat secondary Abs for CD20, CD68 and CD206 or an Omni goat anti-mouse horseradish peroxidase (HRP)-conjugated secondary Ab (Vector laboratory, Burlingame, CA, USA) for CXCL13. All sections were then counterstained with hematoxylin (4 min). Finally, slides were rinsed, manually dehydrated and coverslipped and scanned with the Nanozoomer 2.0 RS (Hamamatsu, Tokyo, Japan). Images of whole tissue areas were captured for analysis using NDPview2 software (Hamamatsu, Tokyo, Japan).

Immunofluorescence

IF analysis was performed on the samples from the same six IPF patients. Whole-slide sections (4 µm) were cut from lung tissue blocks with a microtome, transferred to charged slides, and costained either for CD20 and CXCL13 or for CD68, CD206 and CXCL13 (U DISCOVERY 4 plex IF; Roche Diagnostic, Meylan, France) using the Abs (at similar dilutions) described in the IHC section. Proteins were visualized by incubating sections with unmodified primary Ab with the corresponding HRP-conjugated secondary Ab and then producing the HRP enzyme-mediated deposition of the tyramide-fluorophore that covalently binds to the tissue at the site of the reaction. The primary Ab and secondary Ab-HRP complexes were finally heat-inactivated. CD68 was detected with dicyclohexylcarbodiimide, CD20 and CD206 with fluorescein isothiocyanate, and CXCL13 with cyanine 5. These

sequential reactions were repeated three times. Sections were mounted in fluoromount (Enzo Life Sciences, Farmingdale, NY, USA). All manipulations were performed at the Rennes H2P2 Histopathology platform (SFR UMS CNRS 3480 - INSERM 018). Stained sections were examined by confocal microscopy (Zeiss LSM-880 microscope) at the Rennes Microscopy Rennes Imaging Center (SFR UMS CNRS 3480 - INSERM 018). The recorded images were analyzed using ImageJ software.

Bronchoalveolar lavage (BAL)

BAL was obtained from seven patients with IPF. This study was approved by the local Ethics Committee of Rennes University Hospital (Comité d'éthique, avis n°19.09), and all patients signed written informed consent. Clinical and pulmonary functional data of the seven subjects are presented in Table S1 (see "BAL"). BAL was performed under local anesthesia with 2% lidocaine. A flexible fiberoptic bronchoscope was inserted into the segmental bronchus of the middle lobe or into the lingula. Approximately 100 ml of sterile 0.9% saline was instilled and then collected into sterile propylene tubes. The average volume obtained for experimental research was approximately 10 ml. The resulting BALs were then centrifuged at 150 rpm for 10 min, washed once with 5 ml PBS, and suspended in GlutaMAX RPMI 1640 medium (Thermo Fisher Scientific, France) containing 10% heat-inactivated fetal bovine serum, 2 mM L-glutamine, 20 IU/ml penicillin and 20 µg/ml streptomycin for 3 h. The adherent cells (i.e., AM) were washed and cultured in complete medium in the presence or absence of 20 ng/ml LPS for 24 h. At the end of the treatment, the supernatants were collected and frozen at -20°C. Total RNA was extracted from AM as described below.

Human MoDM culture

Buffy coats and blood samples were collected from healthy donors and from patients with IPF, respectively. All subjects provided consent for their blood to be used for research

(Etablissement Français du Sang, Rennes, France). Clinical and pulmonary functional data of the patients with IPF are presented in Table S1 (see "Blood monocytes"). The peripheral mononuclear cells from buffy coats or from blood samples were collected by Ficoll gradient centrifugation, and monocytes were isolated by adhesion (1 h). The monocytes were then allowed to differentiate into M0 macrophages by incubation (6-7 days) in GlutaMAX RPMI 1640 medium containing 10% heat-inactivated fetal bovine serum, 2 mM L-glutamine, 20 IU/ml penicillin, 20 μg/ml streptomycin and 50 ng/ml M-CSF (16). These resting MoDMs (M0 macrophages) were washed and cultured in fresh complete culture medium containing 10 ng/ml M-CSF. RNA interference technology was used for gene silencing in some experiments. MoDMs were transfected with siRNAs (30 pmol) using Lipofectamine RNAiMAX (Thermo Fisher Scientific, France) according to the manufacturer's instructions and incubated for 24 h with 20 ng/ml M-CSF in complete culture medium before stimulation.

Reverse transcription quantitative polymerase chain reaction (RT-qPCR)

Total RNA was extracted from cells with TRIzol (Thermo Fisher Scientific, France) and reverse transcribed using the High Capacity cDNA Reverse Transcription kit (Applied Biosystems, Thermo Fisher Scientific, France). Quantitative PCR was performed (SYBR Green methodology) on a CFX384 real-time PCR system (BioRad, Marnes-la-Coquette, France) (16). The primers were provided by Sigma-Aldrich (Kiqstart primers). The specificity of amplified genes was checked at the end of PCR using the comparative cycle threshold method (CFX Manager™ Software). These mean Cq values were used to normalize the target mRNA concentrations to those of the 18S ribosomal protein by the $2(-\Delta\Delta Cq)$ method.

Cytokine quantification

The concentrations of CXCL13, TNF-α and IL-10 were measured by ELISA (Duoset ELISA development system kits, R&D Systems Europe, Lille, France) according to the

manufacturer's instructions. The limits of quantification (LOQs) were CXCL13 - 15.2 pg/ml, TNF-α - 13.4 pg/ml, and IL-10 - 31.3 pg/ml. The three cytokines were quantified in cell culture media and in blood serum samples taken from 105 patients when they were diagnosed with IPF. This study was approved by the Ethics Committee related to Rennes University Hospital (Comité de protection des personnes Ouest V, CHU Rennes, n°2014-A00268-39), and each patient signed a written informed consent form. Clinical and pulmonary functional data of the 105 subjects are presented in Table S1 (see "Serum samples"). Serum samples were stored at -80°C at the Biobank, Centre Hospitalier Universitaire, Rennes.

Western blotting

Cells were lysed with RIPA buffer containing a protease inhibitor cocktail (Roche Diagnostic, Meylan, France) and phosphatase inhibitor cocktails 2 and 3 (Sigma-Aldrich, Saint-Quentin Fallavier, France) and then centrifuged. After measuring protein concentrations by the Bio-Rad Protein Assay Kit, the lysates were diluted in loading buffer, heated at 95°C, loaded on a 4% stacking gel and separated on a 10% gel by SDS electrophoresis as previously described (16). The proteins were then transferred to nitrocellulose membranes by electroblotting overnight (30 V at 4°C). After blocking, the membranes were then hybridized overnight at 4°C with appropriate primary Abs and incubated with HRP-conjugated secondary Abs before analysis by chemiluminescence on a ChemiDoc XRS+ System and Image Lab software (Bio-Rad, Marnes-la-Coquette, France). Protein expression was quantified by analyzing each visualized band by densitometry (Image Lab™ Software for total protein normalization; BioRad, Marnes-la-Coquette, France).

Statistical analyses

All cellular endpoints were obtained using AM or MoDM from different donors. The data are reported as the means ± standard deviation (SD). Significant differences were assessed

223 using a two-way Student's *t*-test or a one-way ANOVA followed by the multirange Dunnett's
224 *t*-test for multiple comparisons. For cytokine concentrations in human blood samples,
225 significant differences were assessed using the nonparametric Mann-Whitney test.
226 Correlations between the cytokine blood concentrations were determined using Spearman's
227 rank correlation coefficient. Differences were considered to be significant when $p < 0.05$.
228

Results

CXCL13 is expressed in alveolar macrophages from patients with IPF

We first used IHC to detect CXCL13 in surgical lung biopsies from six patients with IPF. CXCL13 staining was intense around the lymphoid aggregates containing B cells (Figure S1A), which was in agreement with DePianto et al. (7). However, there was no or very weak staining inside B cell aggregates. In addition, IF experiments showed that CXCL13 expression was mostly outside B-cell lymphoid aggregates. Thus, such pulmonary B cells likely do not produce CXCL13 (Figure S1B). We studied CD68 and CD206 expression, which is abundant on pulmonary macrophages from patients with IPF (15), to determine whether CXCL13 was produced by macrophages that had infiltrated the lymphoid aggregates (Figure S1C). There was little CD68 or CD206 staining around or within the lymphoid structures, and CD68/CD206 staining was not colocalized with CXCL13 staining. We therefore looked for CXCL13 in alveolar tissues where macrophages are constitutively present. CD68- and CD206-positive cells (i.e., AM) were abundant in pulmonary alveoli (Figure 1A). These macrophages bore intense CD206 staining. There was CXCL13 staining on most AMs but not on CD68- and CD206-negative cells. The intracellular CXCL13 staining was diffuse, mainly in the cytoplasm but also at the cell membrane. The biopsies from all the patients provided similar images (data not shown). We also stained sections with the CXCL13 isotype control Ab (mouse IgG, Vector, I-2000). The isotype control staining in AM was clearly less intense than the CXCL13 staining (Figure 1A), confirming the specificity of CXCL13 expression in lung biopsies.

Multiplex IF staining showed that CXCL13 was present in CD68- and CD206-positive AM (Figure 1B), while the CD68- and CD206-negative cells in the alveoli had no CXCL13 staining. Similar images were recorded for the five other surgical lung biopsies (Figure S2). This result indicates that AM from patients with IPF likely produces CXCL13.

LPS induces CXCL13 expression by activating NF-κB pathways

We then focused our study on the production of CXCL13 by AM and MoDM. AM were isolated from BAL collected from 7 patients with IPF. AM stimulation with 20 ng/ml LPS for 24 h increased CXCL13 mRNA and CXCL13 protein concentrations in 7 and 4 cell cultures, respectively (Figure 2A). CXCL13 expression was also significantly increased in macrophages differentiated from peripheral blood monocytes of 11 patients with IPF (Figure 2B). It can be noted that the levels of CXCL13 secreted from activated AM were lower than those secreted from "IPF" MoDM. Similarly, CXCL13 mRNA levels were strongly and stably increased in the MoDM of healthy donors stimulated for 8-24 h (Figure 2C, left panel). CXCL13 protein released into the culture medium was maximal after stimulation for 24 h (Figure 2C, right panel). We next examined the signaling pathways mediating CXCL13 gene expression in MoDM. The IκBα kinase inhibitor BAY 11-7082 (BAY) nearly abrogated CXCL13 release from LPS-stimulated MoDM (Figure 2D), which suggests that the NF-κB signaling pathways control CXCL13 gene expression. LPS is known to rapidly activate the canonical NF-κB pathway by stimulating the phosphorylation and subsequent breakdown of the NF-κB inhibitor IκBα, which sequesters NF-κB subunits to the cytoplasm (19). This canonical pathway, activated by the IκB kinase complex, leads to the translocation of the NF-κB dimer RelA:p50 to the nucleus. These transcription factors increase the expression of several genes that regulate innate and adaptive immune responses. The factors also induce the gene encoding IκBα and stimulate the synthesis of the NF-κB subunits NFκB2 (p100) and RelB, which mediate the noncanonical NF-κB pathway. The phosphorylation and subsequent processing of NFκB2 (p100) catalyzed by IκB kinase-α produce the active p52 subunit, which then interacts with RelB (19).

Incubating MoDM with LPS for 2 h stimulated the phosphorylation and breakdown of IκBα followed by increased IκBα synthesis after 24 h (Figure S3A). As expected, pretreatment of MoDM with BAY blocked the stimulation of IκBα synthesis. Incubation with LPS for 24 h also significantly increased the levels of NFκB2 and RelB mRNA (Figure S3B) and the concentrations of the NFκB2 (p100), p52 and RelB proteins in MoDM (Figure S3C). Pretreating cells with BAY completely blocked this late production of the three noncanonical NF-κB subunits (Figure 2E). The fact that CXCL13 synthesis was also delayed in LPS-stimulated human MoDM suggests that the noncanonical NF-κB pathway activated CXCL13 gene transcription, as shown in murine cells (20). We tested this by transfecting MoDM with siRNAs to block RelB mRNA (Si-RelB) and p100/p52 mRNA (Si-p100). Si-RelB completely blocked RelB protein synthesis in LPS-stimulated MoDM but did not affect p100/p52 proteins (Figure 2F and S3D). Si-p100 prevented any increase in p100 and p52 proteins and reduced the expression of RelB protein. This result indicates that transcription of the RelB gene is activated by canonical NF-κB pathways and regulated by noncanonical signaling (21). Blocking the synthesis of RelB or p100/p52 in LPS-stimulated MoDM significantly reduced their CXCL13 mRNA expression levels (Figure 2G). Thus, canonical and noncanonical NF-κB signaling pathways play major roles in the regulation of CXCL13 production by MoDM.

TNF-α and IL-10 mediate CXCL13 gene induction in LPS-stimulated MoDM

We next determined the influence of early LPS-induced cytokines on CXCL13 synthesis by MoDM. We investigated the roles of TNF-α and IL-10 because they were reported to stimulate CXCL13 expression in activated murine stromal cells and LPS-stimulated dendritic cells, respectively (22, 23). LPS rapidly increased the concentrations of both TNF-α and IL-10 mRNAs in MoDM (Figure 3A). Cells stimulated for 4 to 8 h secreted the highest concentration of TNF-α into the culture medium (Figure 3B). In contrast, the amount of IL-10

301 released by cells activated for 24 h gradually increased (Figure 3B). The early induction of
302 both TNF-α and IL-10 genes was fully blocked by BAY (Figure 3C), suggesting that
303 cytokines are involved in CXCL13 synthesis.

304 To explore this hypothesis, we used Abs that neutralized TNF-α (aT) and IL-10 (aI)
305 proteins. aT significantly decreased the amounts of NFκB2 (p100) and RelB mRNAs in
306 MoDM exposed to LPS for 24 h (Figure 3D) and blocked the synthesis of p100/p52 and RelB
307 proteins (Figure 3E). In contrast, aI alone did not modify the amounts of the three
308 noncanonical NF-κB subunits or amplify the effects of aT. However, each Ab alone
309 significantly inhibited both the induction of CXCL13 mRNA in LPS-stimulated MoDM and
310 the secretion of CXCL13 (Figures 3F-G). Interestingly, the aT/aI combination had stronger
311 inhibitory effects on CXCL13 mRNA and CXCL13 protein concentrations than did aT alone
312 (Figure 3F and 3G). These findings suggest that TNF-α mediates CXCL13 gene induction in
313 LPS-stimulated MoDM by activating NF-κB and that IL-10 enhances its effect, leading to
314 maximal CXCL13 synthesis.

315 **IL-10 enhances TNF-α-induced CXCL13 expression by activating JAK/STAT signaling**

316 If TNF-α and IL-10 control CXCL13 gene induction in LPS-stimulated MoDM, human
317 recombinant TNF-α and IL-10 should mimic the effects of LPS in MoDM. Indeed,
318 stimulating MoDM with TNF-α for 24 h but not with IL-10 alone significantly increased both
319 NFκB2 and RelB mRNA levels and p100, p52 and RelB protein expression (Figure 4A-B).
320 The TNF-α/IL-10 combination did not further stimulate the synthesis of the three
321 noncanonical NF-κB subunits (Figure 4B). TNF-α increased CXCL13 mRNA and protein
322 concentrations, and its effect was significantly enhanced by IL-10 (Figure 4C-D). Finally,
323 cells stimulated with IL-10 alone contained slightly increased (up to 12-fold) CXCL13
324 mRNA concentrations and released slightly more CXCL13 (Figures 4C-D). These findings

confirm that TNF-α and IL-10 control CXCL13 expression in MoDM and highlight the fact that IL-10 enhances CXCL13 gene induction independently of any direct NF-κB activation.

The binding of IL-10 to its cognate receptor activates JAK/STAT pathways, rather than NF-κB, and especially stimulates STAT3-dependent signaling in human MoDM (24). We found that LPS increased STAT3 phosphorylation in cells treated for 6 h (Figure S3E) and that the level of phosphorylated STAT3 remained enhanced for 24 h (data not shown). We examined the effects of ruxolitinib, a potent Janus kinase (JAK) inhibitor (25), to determine whether JAK/STAT signaling pathways also mediate CXCL13 synthesis by MoDM. Ruxolitinib blocked the phosphorylation of STAT3 triggered by LPS or IL-10 (Figure S3E). We incubated MoDM with LPS for 4 h to stimulate TNF-α and IL-10 production and then added ruxolitinib for 20 h to block the JAK/STAT pathways. Ruxolitinib did not reduce the secretion of TNF-α or IL-10 (Figure 4E) and did not reduce NFκB2 (p100) or RelB mRNA expression (Figure 4F), which demonstrates that it did not interfere with the NF-κB pathways in MoDM stimulated in these experimental conditions. However, ruxolitinib blocked the increase in CXCL13 mRNA induced by IL-10 (Figure S3F) and LPS (Figure 4G). These results suggest that IL-10 enhances TNF-α-induced CXCL13 expression by activating the JAK/STAT signaling pathway.

TNF-α and IL-10 control LPS-induced CXCL13 gene expression in MoDM and AM from patients with IPF

We then examined whether TNF-α and IL-10 could also control CXCL13 expression in MoDM and AM isolated from patients with IPF. As expected, the treatment of "IPF" MoDM with neutralizing Ab directed against TNF-α and IL-10 significantly reduced the expression of NFκB2, RelB and CXCL13 mRNA levels induced by LPS (Figure 5A). In addition, TNF-α and IL-10 significantly increased CXCL13 mRNA levels (Figure 5B), whereas ruxolitinib

almost completely blocked CXCL13 expression without altering NFκB2 and RelB mRNA levels (Figure 5C). Moreover, incubating AM cultures with LPS for 24 h increased NFκB2 but not RelB mRNA levels, suggesting that the noncanonical NF-κB pathway was not fully activated *in vitro* (Figure 5D). Nevertheless, activated "IPF" AM treated with the aT/aI combination had reduced NFκB2 and CXCL13 mRNA levels (Figure 5D), indicating that TNF-α and IL-10 may also mediate CXCL13 gene expression in activated AM from patients with IPF.

Serum TNF-α and IL-10 concentrations correlate with CXCL13 in patients with IPF

To determine whether TNF-α and IL-10 modulate CXCL13 production in humans, we examined the CXCL13, TNF-α and IL-10 concentrations in blood serum samples taken from 105 patients suffering from IPF at the time of their diagnosis. The arithmetic and median mean concentrations of CXCL13 were 117.94 ± 156.5 pg/ml and 58.6 pg/ml, respectively. Most serum samples had no detectable TNF-α or IL-10 levels. Only 20.9% (n=22) and 13.3% (n=14) of total serum samples had TNF-α or IL-10 concentrations above their LOQ, respectively. Interestingly, almost all the samples with TNF-α or IL-10 concentrations above the LOQ had CXCL13 concentrations higher than the median concentration (Figure 6A; left panel). Moreover, among those samples with TNF-α or IL-10 concentrations above the LOQ, 13/22 (59%) and 8/14 (57.1%) had CXCL13 concentrations in the highest quartile (Figure 6A, right panel), respectively. In addition, the TNF-α concentrations > LOQ (n=22), but not the IL-10 concentrations > LOQ (n=14), significantly correlated with their corresponding CXCL13 concentrations (Figure 6B).

Discussion

In this study, we demonstrated that CXCL13 is expressed in AM and MoDM from patients with IPF. CXCL13 expression was increased *in vitro* in LPS-stimulated AM and MoDM, and was regulated by both canonical and noncanonical NF-κB signaling. LPS rapidly stimulated the expression of TNF-α and IL-10, which then mediate CXCL13 gene induction by activating the NF-κB and JAK/STAT pathways, respectively. TNF-α and IL-10 are also mediators of LPS-induced CXCL13 gene expression in AM. In addition, we show that TNF-α concentrations significantly correlate with the corresponding CXCL13 concentrations in the serum of patients with IPF, suggesting that this major pro-inflammatory cytokine may regulate CXCL13 expression in humans.

IHC confirmed the finding of DePianto et al. (2015) that CXCL13 staining is intense around the B-cell aggregates in lung tissues from patients with IPF (7). The staining was not clear inside the cells, indicating that the protein could be secreted and then deposited on fibrillary structures. Carlsen et al. (2) demonstrated that released CXCL13 is indeed associated with extracellular fibrils such as fibronectin in ulcerative colitis lesions. Our studies also revealed only faint CD68 and CD206 staining around and within B cell aggregates and no colocalization of these markers with CXCL13, indicating that macrophages are probably not the source of CXCL13 in these lymphoid structures. In contrast, our results showed that CD68- and CD206-positive macrophages in pulmonary alveoli contain CXCL13, unlike other cells in these structures. Moreover, stimulating human AM from patients with IPF induced CXCL13 gene expression and CXCL13 release. Thus, pulmonary macrophages are probably a source of CXCL13 in these patients. Nevertheless, we have still to determine whether other pulmonary cells secrete CXCL13 to explain the notably high concentration of CXCL13 around the B-cell aggregates.

Our RNA silencing experiments showed that blocking p100/p52 and RelB synthesis significantly reduced CXCL13 mRNA expression in LPS-stimulated MoDM, confirming that the noncanonical NF-κB pathway contributes significantly to CXCL13 gene expression in human macrophages, as in other murine and human cells (20, 26). However, we did find that optimal CXCL13 gene expression in macrophages required the coordinated activation of the NF-κB pathway by TNF-α and the JAK/STAT pathway by IL-10.

TNF-α activated the noncanonical NF-κB pathway in resting M0 MoDM, unlike IL-10, and only the neutralization of TNF-α blocked NFκB2 and RelB gene induction in LPS-stimulated MoDM. TNF-α alone significantly increased CXCL13 gene expression, and its neutralization prevented the LPS-dependent induction of CXCL13 mRNA. TNF-α activates the canonical NF-κB pathway by binding to the ubiquitous TNF receptor 1, and it also binds to TNF receptor 2 (TNFR2), which triggers p100 processing and activates the noncanonical pathway (27). Nonetheless, the distribution of TNFR2 is considerably more restricted and limited to a few cell types, including human MoDM (28). The processing of p100 is catalyzed by NF-κB-inducing kinase (NIK); it activates IκB kinase-α dimers that, in turn, phosphorylate p100 and trigger its partial breakdown by the proteasome to generate the p52 subunit (29). Basal p100 processing is low in most cells because the TRAF2/TRAF3/cIAP ubiquitin ligase complex constantly mediates ubiquitination and rapid proteasomal breakdown of NIK (29). Activating cells with lymphotoxin-β receptor agonists or TNF-α-induced TNFR2 stimulates TRAF2 breakdown which, in turn, stabilizes NIK protein synthesis and promotes p100 processing. We did not measure NIK production by MoDM, but as the differentiation of monocytes into macrophages increases NIK synthesis (30), the constitutive concentration of stabilized NIK protein was probably sufficient to promote p100 processing.

Neutralizing IL-10 protein did not prevent activation of the noncanonical NF-κB pathway, but it significantly reduced CXCL13 gene expression in LPS-stimulated MoDM. Conversely, IL-10 did not activate NF-κB pathways, although it produced a small increase in the amounts of CXCL13 mRNA in resting MoDM. We interpret these results as demonstrating that IL-10 activates CXCL13 gene expression by an alternative mechanism that is not dependent on NF-κB. The selective JAK inhibitor ruxolitinib significantly reduced the increases in CXCL13 mRNA in both LPS- and IL-10-stimulated MoDM. Ruxolitinib neither prevented the release of TNF-α and IL-10 nor reduced the production of p100/p52 and RelB in activated cells, suggesting that it specifically blocks CXCL13 gene expression by inhibiting the JAK/STAT pathway. We did not further examine this additional pathway, but there is evidence that the transcription factor STAT3 is involved in the effects of LPS and IL-10. First, STAT3 enhances CXCL13 gene expression in other cell types (31); second, LPS and IL-10 activate STAT3 in macrophages (24, 32); and third, we show that ruxolitinib fully blocked the activation of STAT3 induced by LPS and IL-10 in MoDM.

We also found evidence that IL-10 strongly enhanced TNF-α-induced CXCL13 gene expression in MoDM. Stimulating MoDM with TNF-α in combination with IL-10 enhanced the increase in CXCL13 mRNA triggered by TNF-α alone. Moreover, treating MoDM with Abs against both TNF-α and IL-10 reduced CXCL13 gene expression more than incubation with TNF-α alone. This finding suggests that the IL-10-activated JAK/STAT pathway enhances the noncanonical NF-κB-dependent CXCL13 gene expression induced by TNF-α. STAT3 appears to increase the activity of the noncanonical NF-κB pathway by different mechanisms. STAT3 that has been acetylated by the cAMP-response element-binding protein (CREB)-binding protein (CBP)/p300 can enhance p100 processing to p52 in several human cell types (33). However, this phenomenon is unlikely to occur in MoDM, as IL-10 did not

increase the p52 protein concentration induced by TNF-α, and neutralizing IL-10 did not reduce the amount of p52 protein in LPS-stimulated cells. Blocking STAT3 production represses the RelB:p52-dependent induction of the cyclooxygenase 2 gene in human placental cells (34). In this latter study, Yu et al. (2015) showed that STAT3 was colocalized with RelB and p52 in the cytoplasm and nuclei of these cells, suggesting that STAT3 physically interacts with RelB/p52 to increase either their translocation to the nucleus or their transcriptional activity (34). Taken together, these results support the notion that STAT3 cooperates with noncanonical NF-κB to induce maximal CXCL13 gene expression in MoDM. Additional experiments are now warranted to validate this hypothesis. IL-10 may not be involved in the regulation of CXCL13 gene expression only in MoDM; it may also function in dendritic cells, since blocking IL-10 significantly reduced the production of CXCL13 by LPS-stimulated dendritic cells (23). Finally, our data indicate that TNF-α and possibly IL-10 contribute to CXCL13 production in patients with IPF. Stimulating *in vitro* MoDM and AM with LPS increased the expression of the genes encoding NFκB2 and CXCL13, while blocking TNF-α and IL-10 production significantly reduced the increase in CXCL13 mRNA. However, the RelB mRNA concentration in LPS-stimulated AM was not increased. This reduced RelB synthesis may limit the formation of RelB:p52 dimers and consequently the expression of CXCL13 mRNA. Our results clearly show that the amounts of CXCL13 secreted by activated IPF AM in response to LPS stimulation are considerably lower than those released from IPF MoDM. The concentrations of CXCL13 in the blood serum of patients with IPF also provide valuable information. Most blood serum samples that contained CXCL13 concentrations below the median CXCL13 concentration contained no detectable TNF-α or IL-10. In contrast, 48.1% of the serum samples with the highest CXCL13 concentrations (the fourth quartile) had TNF-α concentrations above their LOQ, and 29.6% of these high-CXCL13

samples had similarly high IL-10 concentrations. Moreover, the highest TNF-α concentrations (> LOQ) were strongly correlated with those of CXCL13. As TNF-α controls CXCL13 gene induction *in vitro*, this correlation suggests that the cytokine may also promote CXCL13 production in patients with IPF. In addition, it may be hypothesized that both TNF-α and IL-10 might contribute to CXCL13 expression in lung tissues in patients with IPF. Indeed, TNF-α and IL-10 are present in human lung tissues, and the concentrations of IL-10 mRNA in pulmonary biopsies from patients with IPF are higher than those from controls (35). Bergeron et al. (2003) also reported that hyperplastic alveolar epithelial cells were a prominent source of IL-10 in lung tissues from patients with IPF. TNF-α and IL-10 are also secreted by B and T cells, dendritic cells and macrophages present in lung tissues. We did not investigate why the blood TNF-α and IL-10 concentrations could be quantified in only a small number of IPF patients. However, since TNF-α and IL-10 are typically produced in response to pro-inflammatory stimuli, it seems likely that blood TNF-α, IL-10 and CXCL13 concentrations were especially increased in IPF patients who had inflammation prior to blood sampling. Furthermore, clinical studies on large cohorts will be required to confirm that some patients with IPF have substantial blood TNF and/or IL-10 concentrations and to investigate the clinical consequences of these increased cytokine concentrations.

In conclusion, our results indicate that CXCL13 is produced by AM in patients with IPF and that TNF-α and IL-10 regulate its production. More generally, we identified the crucial roles of the NF-κB and JAK/STAT pathways in CXCL13 gene expression in human inflammatory MoDM.

Acknowledgements

We thank the Microscopy Rennes Imaging Center (MRic) of SFR UMS CNRS 3480 - INSERM 018 for confocal microscopy analyses, Cécile Daoudal (ILD nurse, Centre

Hospitalier Universitaire, Rennes), Mireille Désille (Biobank, Centre Hospitalier Universitaire, Rennes) and Professor Olivier Fardel for helpful comments and critically reading the manuscript. Owen Parkes edited the English text.

Funding

This work was supported by the Institut National de la Santé et de la Recherche Médicale (INSERM), the Université de Rennes (Univ Rennes) and Boehringer Ingelheim Pharma GmbH. Nessrine Bellamri holds a fellowship from the University of Rennes.

References

1. Cyster, J. G., K. M. Ansel, K. Reif, E. H. Ekland, P. L. Hyman, H. L. Tang, S. A. Luther, and V. N. Ngo. 2000. Follicular stromal cells and lymphocyte homing to follicles. *Immunol. Rev.* 176: 181–193.

2. Carlsen, H. S., E. S. Baekkevold, H. C. Morton, G. Haraldsen, and P. Brandtzaeg. 2004. Monocyte-like and mature macrophages produce CXCL13 (B cell-attracting chemokine 1) in inflammatory lesions with lymphoid neogenesis. *Blood* 104: 3021–3027.

3. Litsiou, E., M. Semitekolou, I. E. Galani, I. Morianos, A. Tsoutsa, P. Kara, D. Rontogianni, I. Bellenis, M. Konstantinou, K. Potaris, E. Andreakos, P. Sideras, S. Zakynthinos, and M. Tsoumakidou. 2013. CXCL13 production in B cells via Toll-like receptor/lymphotoxin receptor signaling is involved in lymphoid neogenesis in chronic obstructive pulmonary disease. *Am. J. Respir. Crit. Care Med.* 187: 1194–1202.

4. Finch, D. K., R. Ettinger, J. L. Karnell, R. Herbst, and M. A. Sleeman. 2013. Effects of CXCL13 inhibition on lymphoid follicles in models of autoimmune disease. *Eur. J. Clin. Invest.* 43: 501–509.

5. Klimatcheva, E., T. Pandina, C. Reilly, S. Torno, H. Bussler, M. Scrivens, A. Jonason, C. Mallow, M. Doherty, M. Paris, E. S. Smith, and M. Zauderer. 2015. CXCL13 antibody for the treatment of autoimmune disorders. *BMC Immunol.* 16: 6.

6. Vuga, L. J., J. R. Tedrow, K. V. Pandit, J. Tan, D. J. Kass, J. Xue, D. Chandra, J. K. Leader, K. F. Gibson, N. Kaminski, F. C. Sciurba, and S. R. Duncan. 2014. C-X-C motif chemokine 13 (CXCL13) is a prognostic biomarker of idiopathic pulmonary fibrosis. *Am. J. Respir. Crit. Care Med.* 189: 966–974.

7. DePianto, D. J., S. Chandriani, A. R. Abbas, G. Jia, E. N. N'Diaye, P. Caplazi, S. E. Kauder, S. Biswas, S. K. Karnik, C. Ha, Z. Modrusan, M. A. Matthay, J. Kukreja, H. R. Collard, J. G. Egen, P. J. Wolters, and J. R. Arron. 2015. Heterogeneous gene expression

signatures correspond to distinct lung pathologies and biomarkers of disease severity in idiopathic pulmonary fibrosis. *Thorax* 70: 48–56.

8. Neighbors, M., C. R. Cabanski, T. R. Ramalingam, X. R. Sheng, G. W. Tew, C. Gu, G. Jia, K. Peng, J. M. Ray, B. Ley, P. J. Wolters, H. R. Collard, and J. R. Arron. 2018. Prognostic and predictive biomarkers for patients with idiopathic pulmonary fibrosis treated with pirfenidone: post-hoc assessment of the CAPACITY and ASCEND trials. *Lancet Respir Med* 6: 615–626.

9. Prasse, A., D. V. Pechkovsky, G. B. Toews, W. Jungraithmayr, F. Kollert, T. Goldmann, E. Vollmer, J. Müller-Quernheim, and G. Zissel. 2006. A vicious circle of alveolar macrophages and fibroblasts perpetuates pulmonary fibrosis via CCL18. *Am. J. Respir. Crit. Care Med.* 173: 781–792.

10. Morales-Nebreda, L., A. V. Misharin, H. Perlman, and G. R. S. Budinger. 2015. The heterogeneity of lung macrophages in the susceptibility to disease. *Eur Respir Rev* 24: 505–509.

11. van de Laar, L., W. Saelens, S. De Prijck, L. Martens, C. L. Scott, G. Van Isterdael, E. Hoffmann, R. Beyaert, Y. Saeys, B. N. Lambrecht, and M. Guilliams. 2016. Yolk Sac Macrophages, Fetal Liver, and Adult Monocytes Can Colonize an Empty Niche and Develop into Functional Tissue-Resident Macrophages. *Immunity* 44: 755–768.

12. Gibbons, M. A., A. C. MacKinnon, P. Ramachandran, K. Dhaliwal, R. Duffin, A. T. Phythian-Adams, N. van Rooijen, C. Haslett, S. E. Howie, A. J. Simpson, N. Hirani, J. Gauldie, J. P. Iredale, T. Sethi, and S. J. Forbes. 2011. Ly6Chi monocytes direct alternatively activated profibrotic macrophage regulation of lung fibrosis. *Am. J. Respir. Crit. Care Med.* 184: 569–581.

13. Misharin, A. V., L. Morales-Nebreda, P. A. Reyfman, C. M. Cuda, J. M. Walter, A. C. McQuattie-Pimentel, C.-I. Chen, K. R. Anekalla, N. Joshi, K. J. N. Williams, H. Abdala-

548 Valencia, T. J. Yacoub, M. Chi, S. Chiu, F. J. Gonzalez-Gonzalez, K. Gates, A. P. Lam, T. T.
549 Nicholson, P. J. Homan, S. Soberanes, S. Dominguez, V. K. Morgan, R. Saber, A. Shaffer, M.
550 Hinchcliff, S. A. Marshall, A. Bharat, S. Berdnikovs, S. M. Bhorade, E. T. Bartom, R. I.
551 Morimoto, W. E. Balch, J. I. Sznajder, N. S. Chandel, G. M. Mutlu, M. Jain, C. J. Gottardi, B.
552 D. Singer, K. M. Ridge, N. Bagheri, A. Shilatifard, G. R. S. Budinger, and H. Perlman. 2017.
553 Monocyte-derived alveolar macrophages drive lung fibrosis and persist in the lung over the
554 life span. *J. Exp. Med.* 214: 2387–2404.
555 14. Baran, C. P., J. M. Opalek, S. McMaken, C. A. Newland, J. M. O'Brien, M. G. Hunter, B.
556 D. Bringardner, M. M. Monick, D. R. Brigstock, P. C. Stromberg, G. W. Hunninghake, and
557 C. B. Marsh. 2007. Important roles for macrophage colony-stimulating factor, CC chemokine
558 ligand 2, and mononuclear phagocytes in the pathogenesis of pulmonary fibrosis. *Am. J.*
559 *Respir. Crit. Care Med.* 176: 78–89.
560 15. Yamashita, M., R. Saito, S. Yasuhira, Y. Fukuda, H. Sasamo, T. Sugai, K. Yamauchi, and
561 M. Maemondo. 2018. Distinct Profiles of CD163-Positive Macrophages in Idiopathic
562 Interstitial Pneumonias. *J Immunol Res* 2018: 1436236.
563 16. Bellamri, N., C. Morzadec, A. Joannes, V. Lecureur, L. Wollin, S. Jouneau, and L.
564 Vernhet. 2019. Alteration of human macrophage phenotypes by the anti-fibrotic drug
565 nintedanib. *Int. Immunopharmacol.* 72: 112–123.
566 17. Yu, Y.-R. A., D. F. Hotten, Y. Malakhau, E. Volker, A. J. Ghio, P. W. Noble, M. Kraft, J.
567 W. Hollingsworth, M. D. Gunn, and R. M. Tighe. 2016. Flow Cytometric Analysis of
568 Myeloid Cells in Human Blood, Bronchoalveolar Lavage, and Lung Tissues. *Am. J. Respir.*
569 *Cell Mol. Biol.* 54: 13–24.
570 18. Raghu, G., H. R. Collard, J. J. Egan, F. J. Martinez, J. Behr, K. K. Brown, T. V. Colby, J.-
571 F. Cordier, K. R. Flaherty, J. A. Lasky, D. A. Lynch, J. H. Ryu, J. J. Swigris, A. U. Wells, J.
572 Ancochea, D. Bouros, C. Carvalho, U. Costabel, M. Ebina, D. M. Hansell, T. Johkoh, D. S.

573 Kim, T. E. King, Y. Kondoh, J. Myers, N. L. Müller, A. G. Nicholson, L. Richeldi, M.
574 Selman, R. F. Dudden, B. S. Griss, S. L. Protzko, H. J. Schünemann, and
575 ATS/ERS/JRS/ALAT Committee on Idiopathic Pulmonary Fibrosis. 2011. An official
576 ATS/ERS/JRS/ALAT statement: idiopathic pulmonary fibrosis: evidence-based guidelines for
577 diagnosis and management. *Am. J. Respir. Crit. Care Med.* 183: 788–824.
578 19. Bonizzi, G., and M. Karin. 2004. The two NF-kappaB activation pathways and their role
579 in innate and adaptive immunity. *Trends Immunol.* 25: 280–288.
580 20. Bonizzi, G., M. Bebien, D. C. Otero, K. E. Johnson-Vroom, Y. Cao, D. Vu, A. G. Jegga,
581 B. J. Aronow, G. Ghosh, R. C. Rickert, and M. Karin. 2004. Activation of IKKalpha target
582 genes depends on recognition of specific kappaB binding sites by RelB:p52 dimers. *EMBO J.*
583 23: 4202–4210.
584 21. Bren, G. D., N. J. Solan, H. Miyoshi, K. N. Pennington, L. J. Pobst, and C. V. Paya. 2001.
585 Transcription of the RelB gene is regulated by NF-kappaB. *Oncogene* 20: 7722–7733.
586 22. Suto, H., T. Katakai, M. Sugai, T. Kinashi, and A. Shimizu. 2009. CXCL13 production by
587 an established lymph node stromal cell line via lymphotoxin-beta receptor engagement
588 involves the cooperation of multiple signaling pathways. *Int. Immunol.* 21: 467–476.
589 23. Perrier, P., F. O. Martinez, M. Locati, G. Bianchi, M. Nebuloni, G. Vago, F. Bazzoni, S.
590 Sozzani, P. Allavena, and A. Mantovani. 2004. Distinct transcriptional programs activated by
591 interleukin-10 with or without lipopolysaccharide in dendritic cells: induction of the B cell-
592 activating chemokine, CXC chemokine ligand 13. *J. Immunol.* 172: 7031–7042.
593 24. Staples, K. J., T. Smallie, L. M. Williams, A. Foey, B. Burke, B. M. J. Foxwell, and L.
594 Ziegler-Heitbrock. 2007. IL-10 induces IL-10 in primary human monocyte-derived
595 macrophages via the transcription factor Stat3. *J. Immunol.* 178: 4779–4785.

25. Febvre-James, M., V. Lecureur, Y. Augagneur, A. Mayati, and O. Fardel. 2018. Repression of interferon β-regulated cytokines by the JAK1/2 inhibitor ruxolitinib in inflammatory human macrophages. *Int. Immunopharmacol.* 54: 354–365.

26. Tando, T., A. Ishizaka, H. Watanabe, T. Ito, S. Iida, T. Haraguchi, T. Mizutani, T. Izumi, T. Isobe, T. Akiyama, J. Inoue, and H. Iba. 2010. Requiem protein links RelB/p52 and the Brm-type SWI/SNF complex in a noncanonical NF-kappaB pathway. *J. Biol. Chem.* 285: 21951–21960.

27. Borghi, A., L. Verstrepen, and R. Beyaert. 2016. TRAF2 multitasking in TNF receptor-induced signaling to NF-κB, MAP kinases and cell death. *Biochem. Pharmacol.* 116: 1–10.

28. Ruspi, G., E. M. Schmidt, F. McCann, M. Feldmann, R. O. Williams, A. A. Stoop, and J. L. E. Dean. 2014. TNFR2 increases the sensitivity of ligand-induced activation of the p38 MAPK and NF-κB pathways and signals TRAF2 protein degradation in macrophages. *Cell. Signal.* 26: 683–690.

29. Sun, S.-C. 2011. Non-canonical NF-κB signaling pathway. *Cell Res.* 21: 71–85.

30. Li, T., M. J. Morgan, S. Choksi, Y. Zhang, Y.-S. Kim, and Z. Liu. 2010. MicroRNAs modulate the noncanonical transcription factor NF-kappaB pathway by regulating expression of the kinase IKKalpha during macrophage differentiation. *Nat. Immunol.* 11: 799–805.

31. Eddens, T., W. Elsegeiny, M. de la L. Garcia-Hernadez, P. Castillo, G. Trevejo-Nunez, K. Serody, B. T. Campfield, S. A. Khader, K. Chen, J. Rangel-Moreno, and J. K. Kolls. 2017. Pneumocystis-Driven Inducible Bronchus-Associated Lymphoid Tissue Formation Requires Th2 and Th17 Immunity. *Cell Rep* 18: 3078–3090.

32. Agbanoma, G., C. Li, D. Ennis, A. C. Palfreeman, L. M. Williams, and F. M. Brennan. 2012. Production of TNF-α in macrophages activated by T cells, compared with lipopolysaccharide, uses distinct IL-10-dependent regulatory mechanism. *J. Immunol.* 188: 1307–1317.

621 33. Nadiminty, N., W. Lou, S. O. Lee, X. Lin, D. L. Trump, and A. C. Gao. 2006. Stat3
622 activation of NF-{kappa}B p100 processing involves CBP/p300-mediated acetylation. *Proc.*
623 *Natl. Acad. Sci. U.S.A.* 103: 7264–7269.
624 34. Yu, L. J., B. Wang, N. Parobchak, N. Roche, and T. Rosen. 2015. STAT3 cooperates with
625 the non-canonical NF-κB signaling to regulate pro-labor genes in the human placenta.
626 *Placenta* 36: 581–586.
627 35. Bergeron, A., P. Soler, M. Kambouchner, P. Loiseau, B. Milleron, D. Valeyre, A. J.
628 Hance, and A. Tazi. 2003. Cytokine profiles in idiopathic pulmonary fibrosis suggest an
629 important role for TGF-beta and IL-10. *Eur. Respir. J.* 22: 69–76.
630
631

Figure Legends

Figure 1: CXCL13 is expressed in CD68- and CD206-positive AM. The lung tissue from a patient with IPF was explored for CD68, CD206 and CXCL13 by IHC (A) and IF (B). (B) upper panels: x 65. Red circles indicate the regions at higher magnifications. Red arrowheads indicate cells negative for CD68/CD206 and CXCL13. IHC was also performed using the CXCL13 isotype control Ab to confirm specific CXCL13 expression in AM. Similar images of CD68, CD206 and CXCL13 staining by IHC were obtained with lung tissues from six patients with IPF.

Figure 2: CXCL13 expression is induced in activated AM and MoDM and is controlled by NF-κB. AM and MoDM from patients with IPF (A, B) and MoDM from healthy donors (C-G) were cultured without (M0) or with 20 ng/ml LPS for 24 h or other indicated times. In some experiments, MoDMs were first treated with 5 µM Bay (C-E) or transiently transfected with control, RelB or p100/p52 siRNA for 24 h (F-G). Relative CXCL13 mRNA was measured by quantitative RT-PCR and normalized to endogenous ribosomal 18S RNA levels. Data are expressed relative to mRNA levels found in cells stimulated with LPS (A, B), in M0 cells (C) or in cells transfected with control siRNA (SiC) and stimulated with LPS (G), arbitrarily set at 1. CXCL13 concentrations in cultured media were measured by ELISA. In (E-F), cells were lysed, and protein expression was analyzed by Western blotting. Protein expression was quantified by analyzing each visualized band by densitometry. The results are the means ± SD of 7 (A), 11 (B), 4 (C, left panel), 5 (C, right panel), 4 (D), 4 (E), and 7 (G) independent experiments. *p<0.05, **p<0.01, ***p<0.001 versus LPS (A, B), M0 (C) "0" LPS (D, E) and "SiC" LPS (G)

Figure 3: CXCL13 expression is mediated by TNF-α and IL-10 in LPS-stimulated MoDM. MoDMs were untreated (M0, 0) or treated with 5 µM BAY or 2 µg/ml neutralizing

Abs directed against TNF-α (aT) or IL-10 (aI) and then stimulated with 20 ng/ml LPS for 1 h (C), 24 h (D-G) or the indicated times (A, B). Relative mRNA levels were determined by quantitative RT-PCR and normalized to endogenous ribosomal 18S mRNA levels. Data are expressed relative to mRNA levels found in M0 cells (A) or cells stimulated with "0" LPS (C, D, F), arbitrarily set at 1. Concentrations of TNF-α, IL-10 and CXCL13 secreted in the culture media were quantified by ELISA. In (E), cells were lysed, and protein expression was analyzed by Western blotting. Protein levels were quantified by analyzing each visualized band by densitometry. The results are expressed as the means ± SD of 7 (A), 5 (B), 3 (C), 3 (D left panel), 7 (D, right panel), 4 (E), 7 (F) and 5 (G) independent experiments. *p<0.05, **p<0.01, ***p<0.001 versus "M0" (A, B), "0" LPS (C-G).

Figure 4: IL-10 enhances CXCL13 expression induced by TNF-α through the JAK/STAT pathway. MoDMs were untreated (M0) or stimulated with 20 ng/ml TNF-α (T) and/or IL10 (I) for 24 h or with 20 ng/ml LPS for 24 h. In (B), cells were lysed, and protein expression was analyzed by Western blotting. Protein levels were quantified by analyzing each visualized band by densitometry. Relative mRNA levels were determined by quantitative RT-PCR and normalized to endogenous ribosomal 18S RNA levels. Data are expressed relative to mRNA levels found in M0 cells (A, C) or in cells stimulated with "0" LPS (F-G), arbitrarily set at 1. Concentrations of TNF-α, IL10 and CXCL13 secreted in the culture media were quantified by ELISA. The results are expressed as the means ± SD of 6 (A, left panel), 4 (A, right panel), 7 (B), 9 (C), 6 (D), 4 (E), 5 (F-G)) independent experiments. *p<0.05, **p<0.01, ***p<0.001 versus M0 (A-D) or "0" LPS (E-G).

Figure 5: Effects of neutralizing Abs directed against TNF-α (aT) or IL-10 (aI) on AM. MoDM (A-C) and AM (D) from patients with IPF were untreated (0) or treated with 2 µg/ml aT and/or aI and then stimulated with 20 ng/ml T/I or 20 ng/ml LPS for 24 h. Relative mRNA

levels were determined by quantitative RT-PCR and normalized to endogenous ribosomal 18S RNA levels. Data are expressed relative to mRNA levels found in cells stimulated with "0" LPS, arbitrarily set at 1. The results are expressed as the means ± SD of 11 (A) and 4 (B-D) independent experiments. *p<0.05, **p<0.01, ***p<0.001 versus "0" LPS (A, C-D) or M0 (B).

Figure 6: TNF-α, IL-10 and CXCL13 concentrations in the serum of patients with IPF. Concentrations of TNF-α, IL-10 and CXCL13 in the blood serum of 105 patients with IPF were measured by ELISA. In (A), TNF-α and IL-10 concentrations were referred to CXCL13 median "M" (A, left panel) or quartiles "Q" (A, right panel). The numbers of values of TNF-α or IL-10 concentrations above their respective LOQs are indicated in italics. (B) Correlations between the values of the blood serum concentrations of CXCL13 and those of TNF-α and IL10 above their respective LOQs. *r_s: Spearman's rank correlation coefficient; ns: not significant.* ***p<0.001

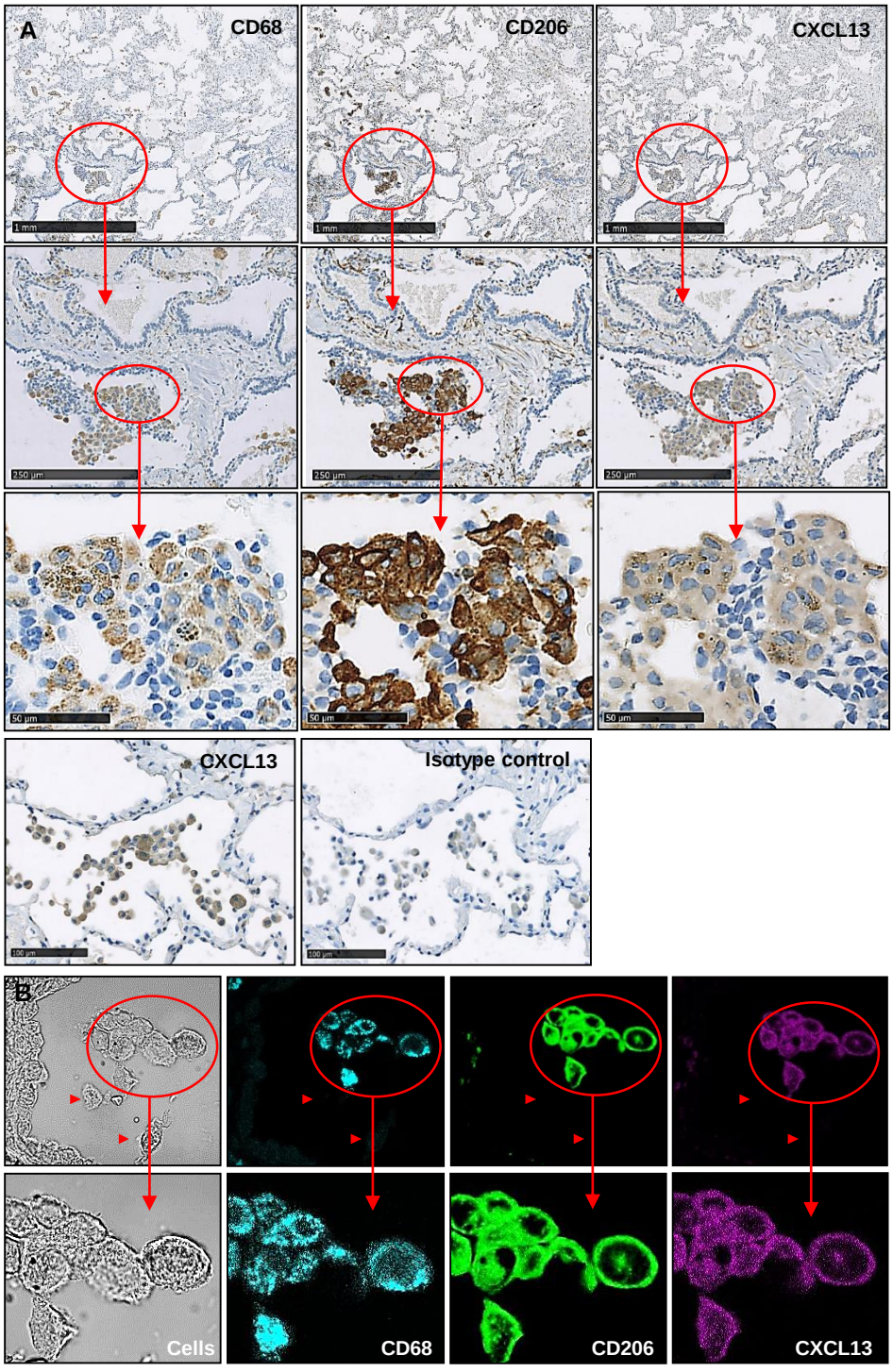
A
CD68
CD206
CXCL13
1 mm
250 µm
50 µm
CXCL13
Isotype control
100 µm
B
Cells
CD68
CD206
CXCL13

Figure 1

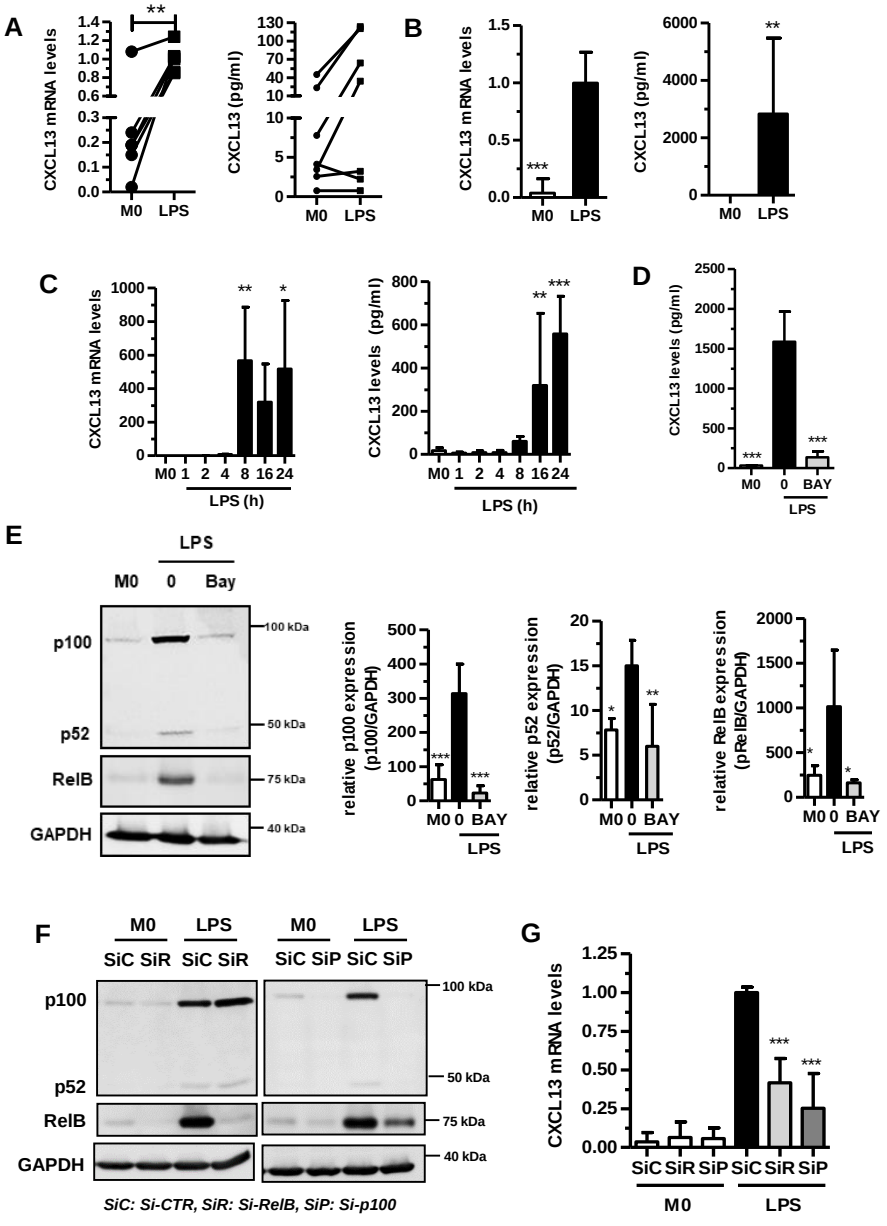
A
CXCL13 mRNA levels
CXCL13 (pg/ml)
M0 LPS
B
C
CXCL13 mRNA levels
CXCL13 levels (pg/ml)
M0 1 2 4 8 16 24
LPS (h)
D
M0 0 BAY
LPS
E
LPS
M0 0 Bay
p100
p52
RelB
GAPDH
100 kDa
50 kDa
75 kDa
40 kDa
relative p100 expression (p100/GAPDH)
relative p52 expression (p52/GAPDH)
relative RelB expression (pRelB/GAPDH)
F
M0 LPS M0 LPS
SiC SiR SiC SiR SiC SiP SiC SiP
SiC: Si-CTR, SiR: Si-RelB, SiP: Si-p100
G
SiC SiR SiP SiC SiR SiP
M0 LPS

Figure 2

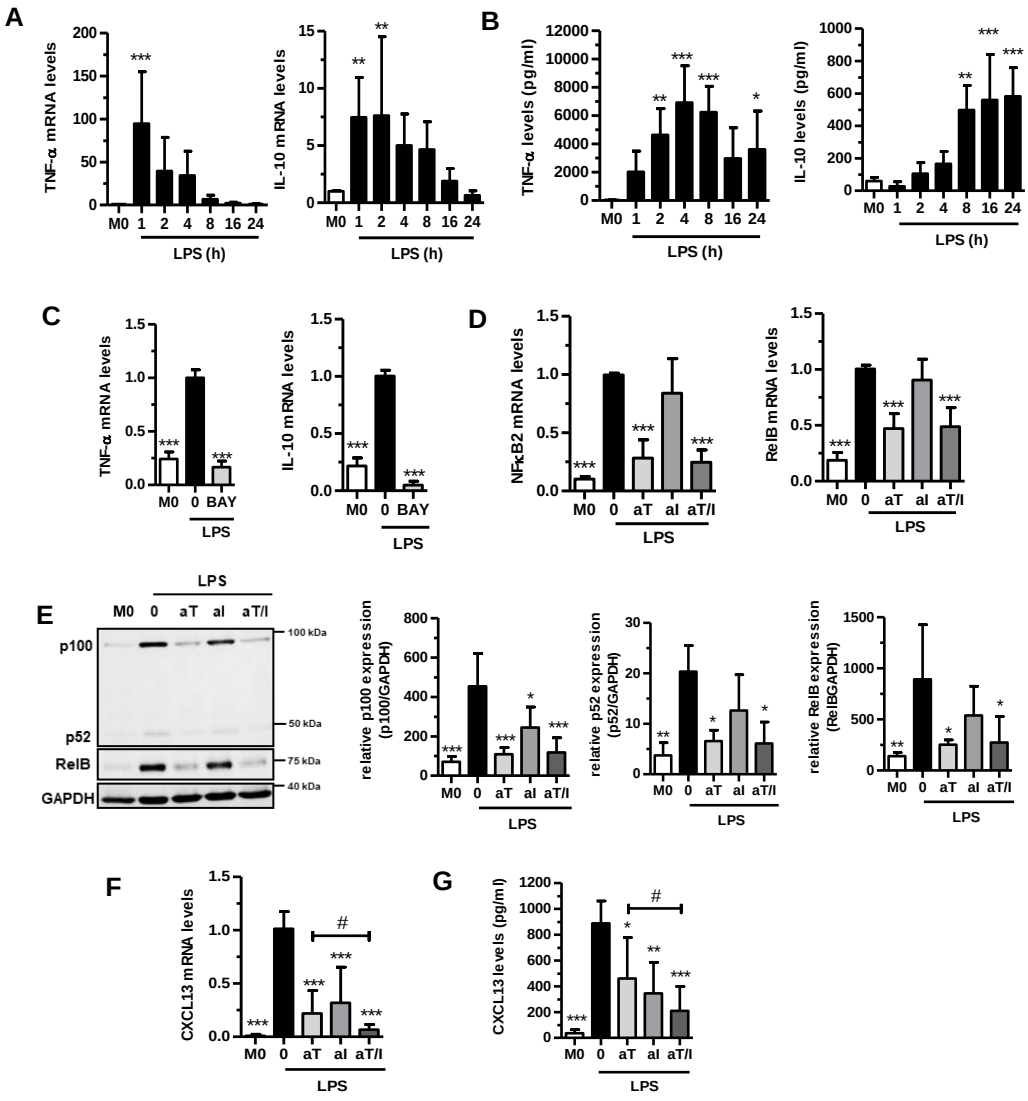
A
TNF-α mRNA levels
IL-10 mRNA levels
M0 1 2 4 8 16 24
LPS (h)
B
TNF-α levels (pg/ml)
IL-10 levels (pg/ml)
C
BAY
LPS
D
NFκB2 mRNA levels
RelB mRNA levels
M0 0 aT aI aT/I
E
p100
p52
RelB
GAPDH
100 kDa
50 kDa
75 kDa
40 kDa
relative p100 expression (p100/GAPDH)
relative p52 expression (p52/GAPDH)
relative RelB expression (RelBGAPDH)
F
CXCL13 mRNA levels
G
CXCL13 levels (pg/ml)

Figure 3

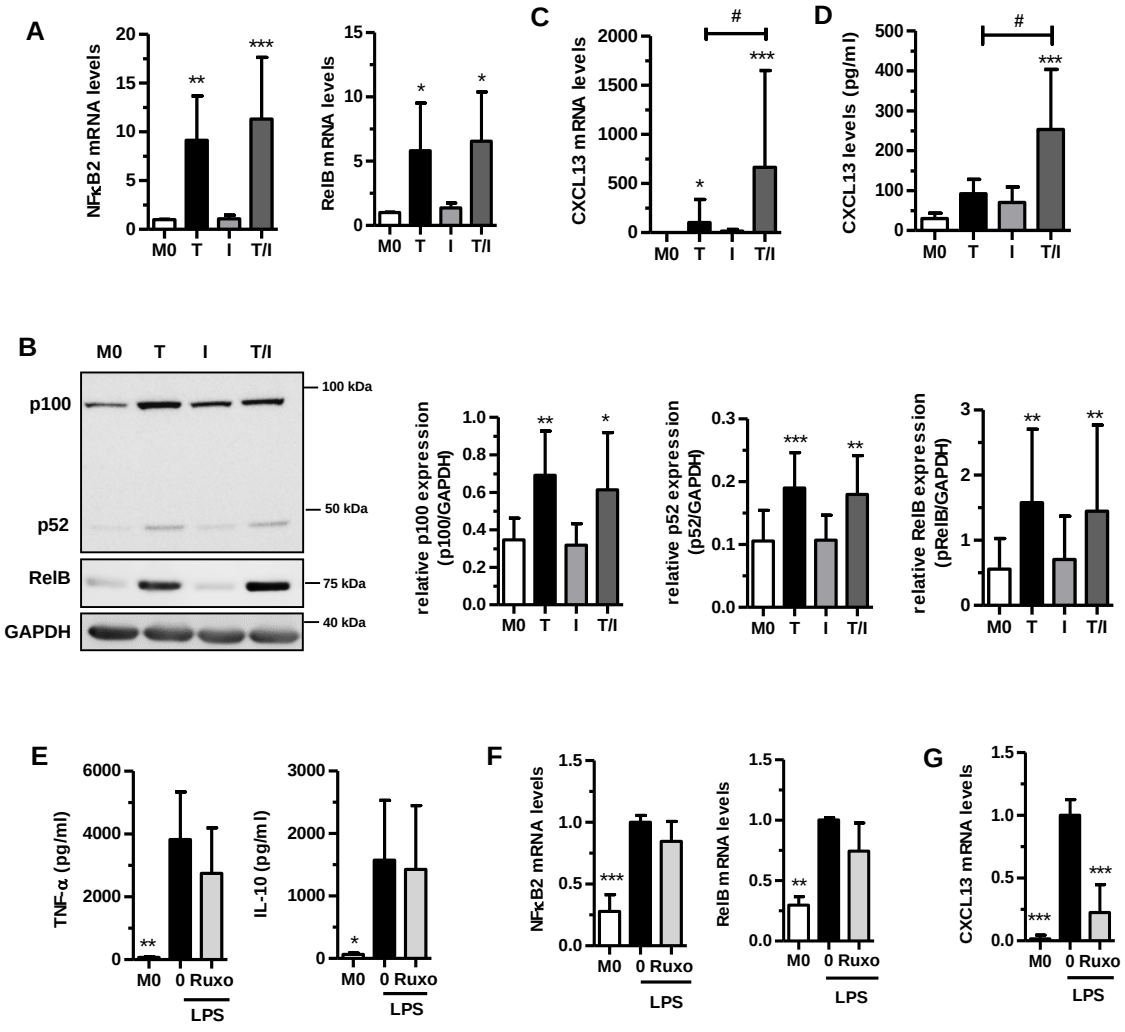
A
NFκB2 mRNA levels
RelB mRNA levels
M0 T I T/I
C
CXCL13 mRNA levels
D
CXCL13 levels (pg/ml)
B
M0 T I T/I
p100
p52
RelB
GAPDH
100 kDa
50 kDa
75 kDa
40 kDa
relative p100 expression (p100/GAPDH)
relative p52 expression (p52/GAPDH)
relative RelB expression (pRelB/GAPDH)
E
TNF-α (pg/ml)
IL-10 (pg/ml)
M0 0 Ruxo
LPS
F
NFκB2 mRNA levels
RelB mRNA levels
G
CXCL13 mRNA levels

Figure 4

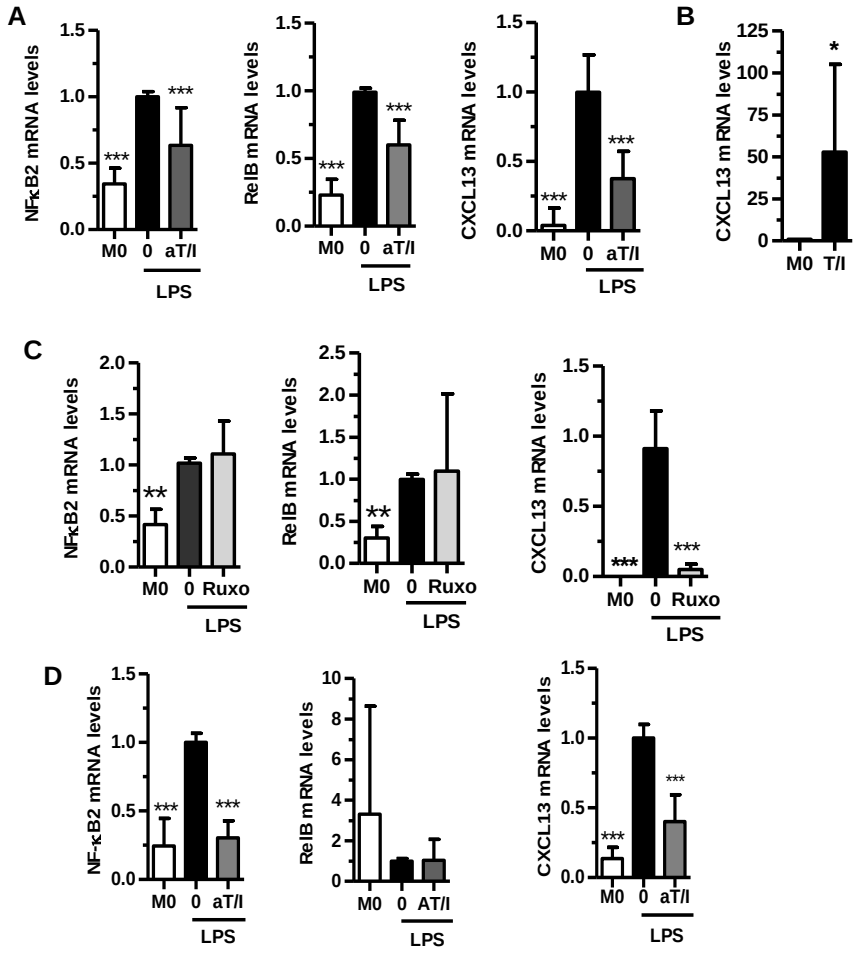
A
NFκB2 mRNA levels
RelB mRNA levels
CXCL13 mRNA levels
M0
0
aT/I
LPS
B
CXCL13 mRNA levels
M0
T/I
C
NFκB2 mRNA levels
RelB mRNA levels
CXCL13 mRNA levels
M0
0
Ruxo
LPS
D
NF-κB2 mRNA levels
RelB mRNA levels
CXCL13 mRNA levels
M0
0
aT/I
AT/I
LPS

Figure 5

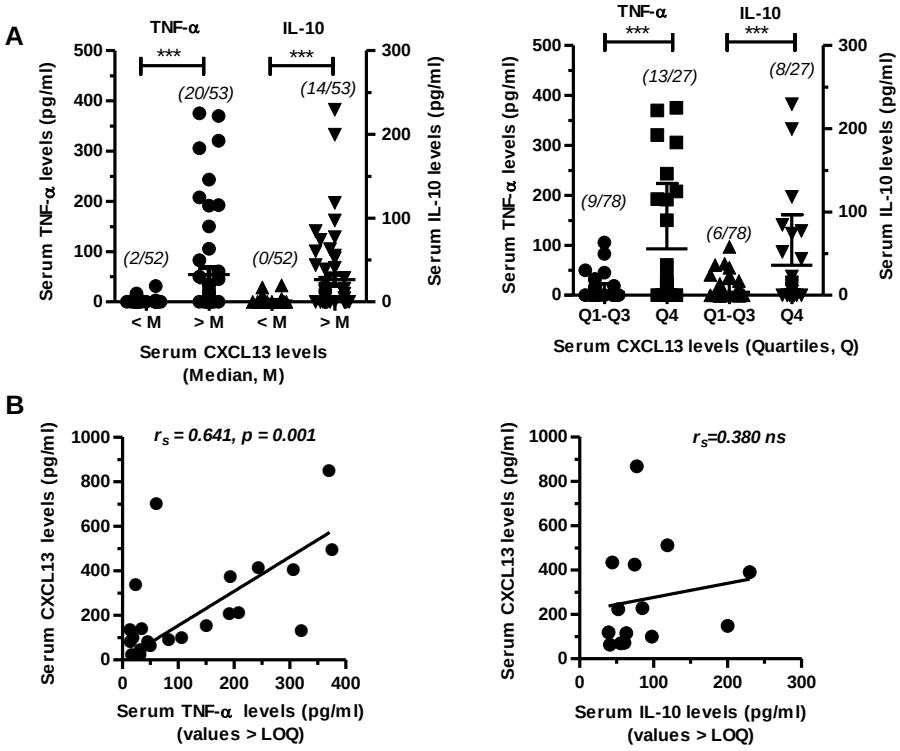
A
TNF-α
IL-10
***
***
(20/53)
(14/53)
(2/52)
(0/52)
Serum TNF-α levels (pg/ml)
Serum IL-10 levels (pg/ml)
< M
> M
< M
> M
Serum CXCL13 levels
(Median, M)
TNF-α
IL-10
***
***
(13/27)
(8/27)
(9/78)
(6/78)
Q1-Q3
Q4
Q1-Q3
Q4
Serum CXCL13 levels (Quartiles, Q)
B
r_s = 0.641, p = 0.001
Serum CXCL13 levels (pg/ml)
Serum TNF-α levels (pg/ml)
(values > LOQ)
r_s=0.380 ns
Serum IL-10 levels (pg/ml)
(values > LOQ)

Figure 6

Table S1. Clinical and functional characteristics of patients with IPF

Variable	Mean (SD) unless otherwise specified			
	Lung biopsies	BAL	Blood monocytes	Serum samples
Number of patients	6	7	11	105
Sex (M:F)	6:0	6:1	10:1	80:25
Age at diagnosis (years)	70.0 (5.1)	75.6 (10.1)	73.8 (8.3)	75.0 (7.9)
Smoker (Y:N)	3:3	4:3	8:3	67:38
BMI (kg/m²)	28.3 (2.0)	28.2 (2.9)	25.5 (2.5)	26.5 (3.8)
FVC % predicted	74.5 (15.6)	85.2 (19.1)	78.7 (13.3)	82.0 (16.7)
DLco % predicted	46.5 (10.9)	50.6 (11.9)	52.5 (14.1)	43.8 (13.6)
Treatment (no:pirf/nint)	6:0	1:6	3:8	105:0

M:F: male:female; BAL: bronchoalveolar lavages; BMI: body mass index; FVC: forced vital capacity, DLco: diffusion capacity for carbon monoxide; pirf/nint: pirfenidone or nintedanib

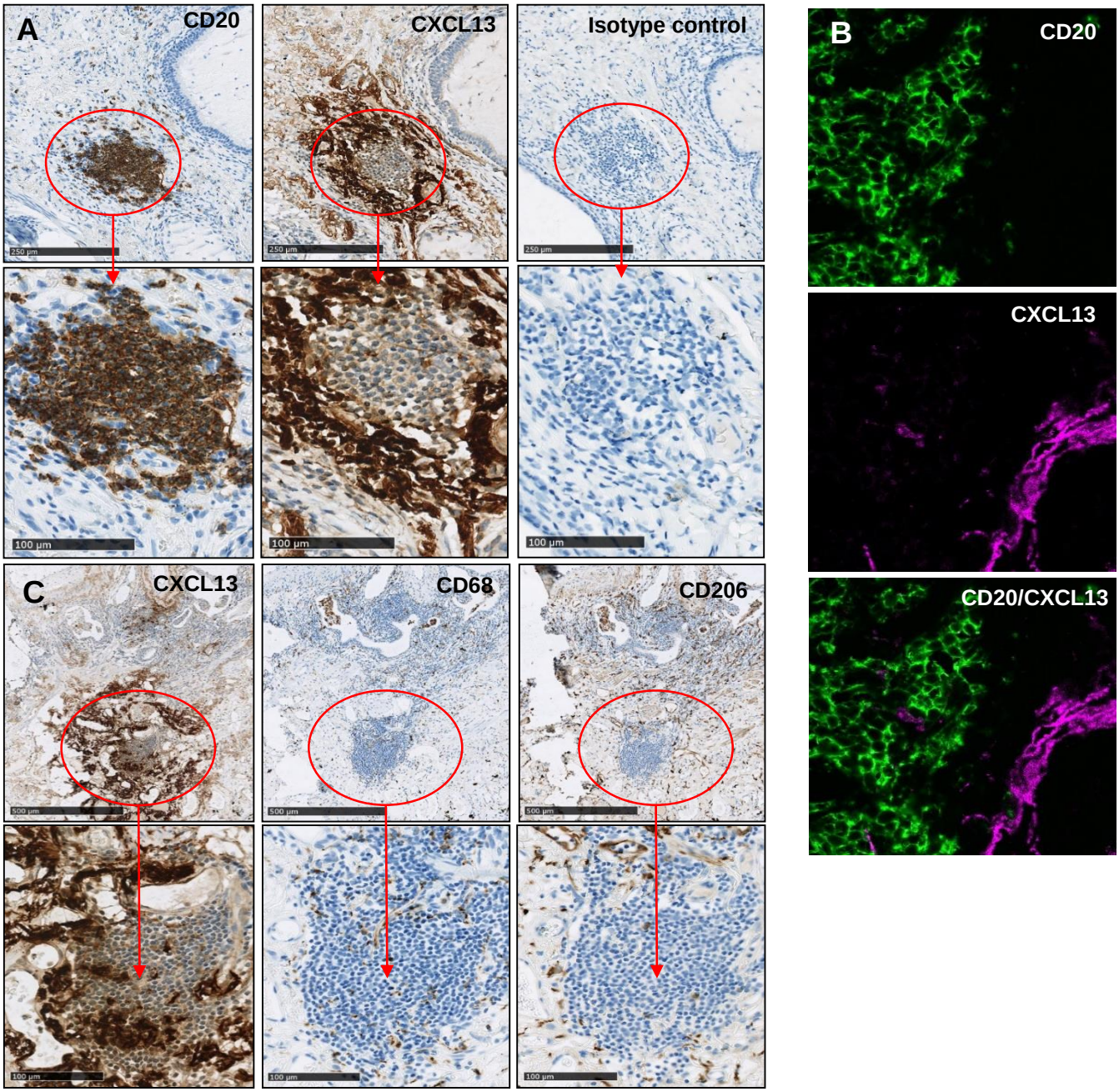

Figure S1: Expression of CXCL13 (A, C), CD68 and CD206 (C) around or within CD20-positive lymphoid aggregates on surgical lung biopsy isolated from a patient with IPF were analyzed by IHC as described in the "Materials and methods" section. Immunostaining was also performed using the CXCL13 isotype control Ab (A). Red circles indicate the region shown at a higher magnification in panels (A, C) . (B) IF staining was performed to confirm CXCL13 expression inside and around CD20-positive lymphoid aggregates, as described in the "Materials and method" section. Similar images of CXCL13, CD68 and CD206 staining by IHC were obtained with lung tissues isolated from six patients with IPF.

Figure S1

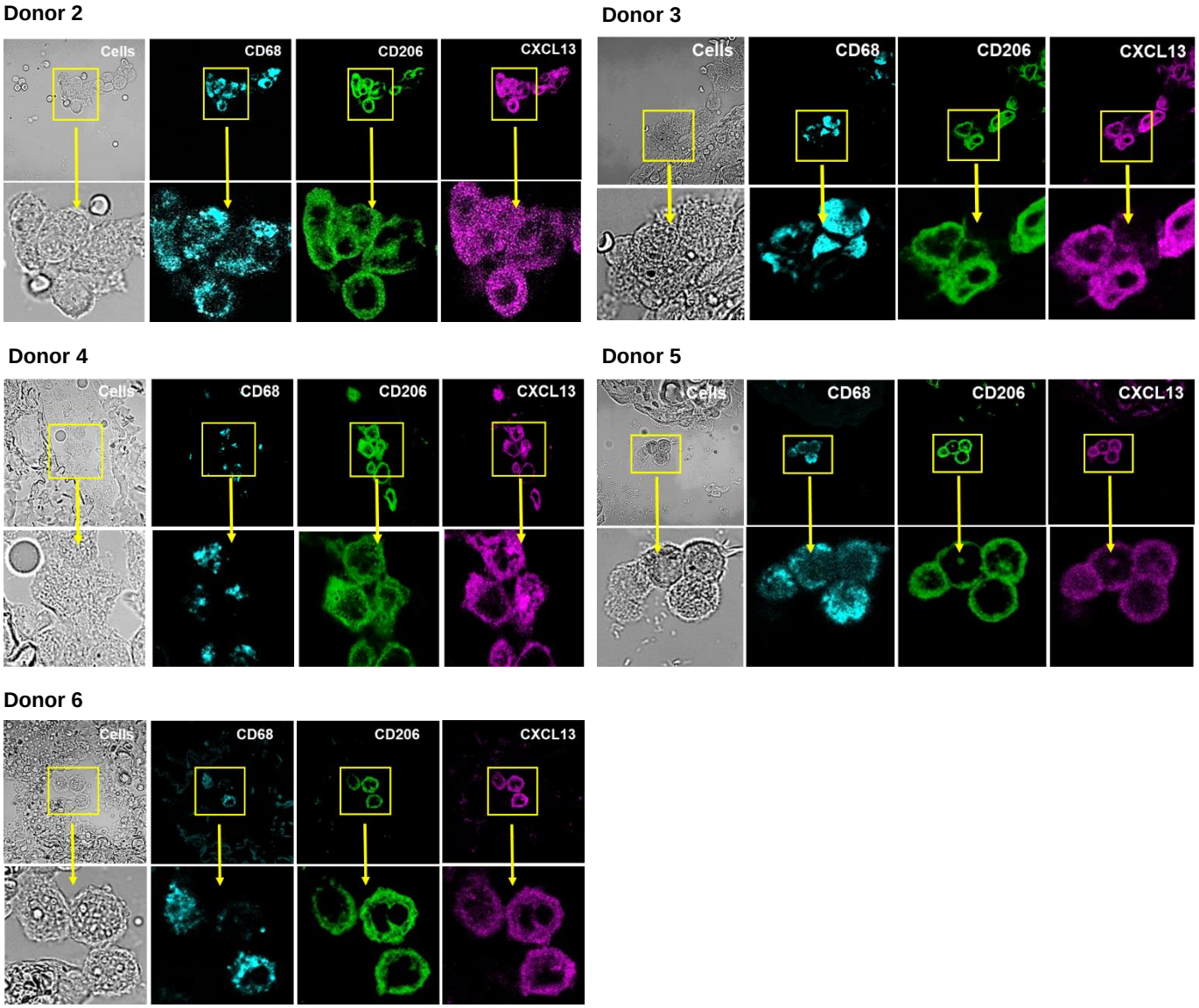

Figure S2: Expression of CD68, CD206 and CXCL13 in alveolar tissues isolated from five different patients with IPF. Multiplex IF staining was performed as described in the "Materials and method" section. Yellow squares indicate the region shown at a higher magnification in the panels.

Figure S2

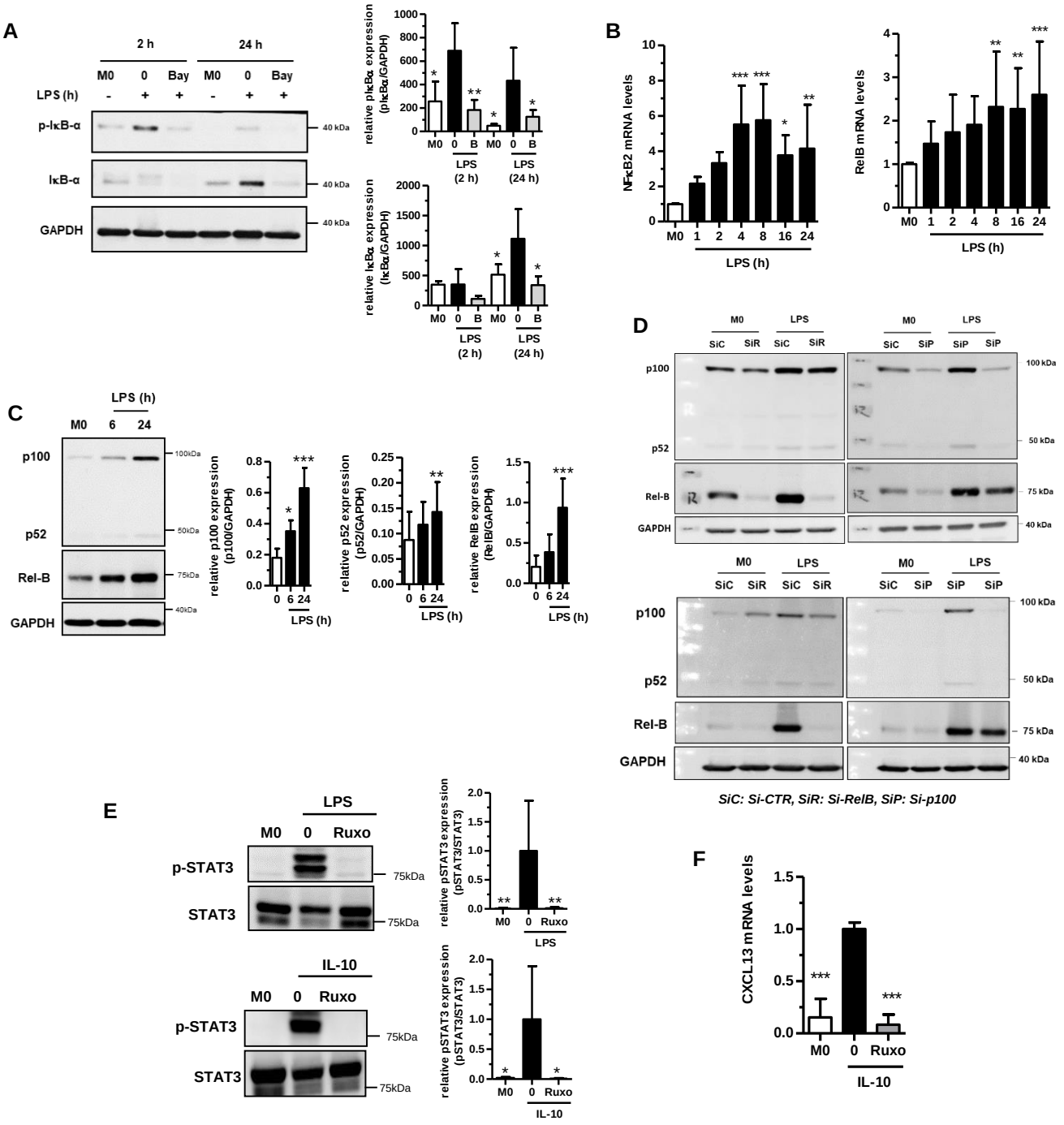

Figure S3: Human MoDM were left untreated (M0) or treated with 5 µM BAY 11-7082 (BAY) (A) or 5 µM ruxolitinib (Ruxo) (E, F) and then stimulated either with 20 ng/ml LPS for 6 h (E) or for the indicated times (A-C), or with 10 ng/ml IL-10 for 10 min (E) or 24 h (F). In (D), two independent cell cultures were transiently transfected with control, RelB or p100/p52 SiRNA for 24 h and then stimulated with 20 ng/ml LPS for 24 h. In (A, C-E), cell were lysed and total proteins were extracted as described in Materials and Methods. Protein expressions were determined by Western blotting and the visualized bands were analyzed by densitometry using Image Lab™ Software for total protein normalization (BioRad, Marnes-la-Coquette, France). In (B, F), relative mRNA levels were determined by quantitative RT-PCR and normalized to endogenous ribosomal 18S RNA levels. Data are expressed relative to mRNA levels found in M0 cells (B) or "0" IL-10 (F), arbitrarily set at 1. Results are expressed as means ± SD of 4 (A, C, E lower panel), 6 (B, E upper panel) and 3 (F) independent experiments. *p<0.05, **p<0.01, ***p<0.001 versus 0 "LPS" (A, E upper panel), M0 (B, C) or "0" IL-10 (E lower panel, F).

Figure S3